# CARBIDE PRECIPITATION IN SOME SECONDARY HARDENED STEELS

A.D.B.Gingell[1] , D. G. Jones[2],
K. J. A. Mawella[2] and H.K.D.H.Bhadeshia[1]

ABSTRACT

The precipitation of alloy carbides in three commercial quenched and tempered martensitic steel has been studied using phase stability calculations, microscopy, microanalytsis and dilatometry. The sequence of carbide stability as estimated using the phase stability calculations is found to be consistent with the microstructural observations, if it is assumed that the equilibrium $M_{23}C_6$ phase is suppressed by kinetic considerations. One interesting result is that the molybdenum-rich phase $M_2C$ is neither predicted nor observed in any of the alloys, all of which contain substantial quantities of molybdenum. Other results include dilatometric experiments which enabled the measurement of transformation temperatures, which are compared against what is expected theoretically.

## 1. INTRODUCTION

Martensitic steels usually have to be tempered in order to obtain an optimum combination of strength and toughness. The tempering process usually leads to a decrease in strength due to the precipitation of iron carbides from carbon that was originally in solid solution in the martensite. However, when the steel contains strong carbide-forming elements such as molybdenum, vanadium and chromium, it becomes possible to recover the strength during prolonged tempering at elevated temperatures. This is called *secondary hardening* - it occurs because substitutional alloying elements (such as Cr) can diffuse during prolonged annealing to precipitate finely dispersed alloy carbides [see for example, reference 1].

The alloy carbides found in secondary-hardened steels are thermodynamically more stable than iron carbides and show little tendency to coarsen. However, many of the

[1] Cambridge University, Materials Science and Metallurgy, Pembroke St., Cambridge CB2 3QZ, U. K.
[2] Defence Research Agency, Fort Halstead, Kent.

alloy carbides find it difficult to nucleate, so that the equilibrium carbide is not necessarily the first to precipitate. Instead, there is a sequence of alloy carbides precipitated in an order determined by a combination of kinetic and thermodynamic considerations, but which leads ultimately towards an equilibrium microstructure. The aim of the present work was to investigate the precipitation of alloy carbides during the tempering of three high strength secondary hardended steels with slightly different chemical compositions. The steels are a part of a programme of research aimed at the optimisation of strength and toughness.

## 2. EXPERIMENTAL

### 2.1. Material

The three steels investigated were provided by the Defence Research Agency, Fort Halstead. They were supplied in standard (steel 1), high purity (steel 2) and modified high purity (steel 3) forms. Their compositions are given in table 1.

| | C | S | P | Si | Mn | Ni | Cr | Mo | V |
|---|---|---|---|---|---|---|---|---|---|
| Steel 1 | 0.33 | 0.003 | <0.002 | 0.24 | 0.44 | 3.33 | 0.93 | 0.65 | 0.20 |
| Steel 2 | 0.31 | 0.002 | 0.003 | 0.03 | 0.01 | 3.56 | 0.98 | 0.96 | 0.18 |
| Steel 3 | 0.38 | 0.002 | <0.01 | <0.05 | <0.03 | 3.65 | 1.23 | 1.54 | 0.21 |

Table 1. Chemical compositions of steels (wt%).

Steel 1 is a conventional secondary hardening alloy produced commercially, with deliberate additions of manganese and silicon. These elements have little effect on the secondary hardening but are known to embrittle steels through segregation to the austenite grain boundaries [2]. Consequently their removal should improve toughness. Steel 2 is a high purity steel with a similar composition to steel 1 but with manganese and silicon removed. Finally, steel 3 is also a high purity steel but with a higher concentration of carbon and alloying elements to give a greater fraction of carbides in the final microstructure.

## 2.2. Thermodynamic Modelling

Equilibrium phase diagram calculations were carried out using MTDATA [3], taking into account the following components and phases (the *M* in each of the carbide phases refers to metal atoms, and the *a* represents ferrite):

System components: $Fe$, $C$, $Mn$, $Si$, $Mo$, $V$, $Ni$, $Cr$

System phases: ferrite, $M_2C$, $M_3C$, $M_7C_3$, $M_{23}C_6$, $M_6C$, $a$

The calculations were conducted for a temperature of 560 °C, corresponding to the tempering temperature used commerciallyl. The sequence of thermodynamic stability can be examined by first conducting the calculations with all phases permitted. The supression from the calculation of the carbide phase which is found to be dominant then allows the next most stable phase to appear, so that a sequence of carbide precipitation based on thermodynamic stability can be determined.

## 2.3.Microscopy

Thin foil transmission electron microscopy (TEM) was carried out to characterise the actual microstructures that develop on tempering. The three alloys were austenised at 870 °C for 2 hours, water quenched to room temperature and tempered at 560 °C for varying lengths of time, from 1 to 16 hours. All heat treatments were carried out with the samples sealed in evacuated silica tubes in order to prevent oxidation and decarburisation of the steels. Microscopy was conducted using a Philips 400 TEM operating at 120 kV using bright field and dark field imaging and selected area diffraction patterns to identify carbides. Microanalysis has also been used to confirm the substitutional solute content of the carbides.

## 2.4. Dilatometry

Austenite formation begins during heating at the $Ac_1$ temperature and is completed when the $Ac_3$ temperature is reached The latter temperature naturally defines the lower limit of the austenisation temperature. Tempering must be carried out below the $Ac_1$ temperature because the partial formation of austenite during tempering would lead to the formation of brittle untempered martensite on cooling. The austenite formation temperatures were therefore determined using dilatometry and compared with theoretical estimates based on the alloy composition. The experiments also allowed a

direct measurement of the martensite-start temperatures during cooling from the austenitic state. These were compared against calculated values.

The dilatometry was carried out using a *Thermecmastor* thermomechanical simulator. Cylindrical specimens 12 mm in height and 8 mm in diameter were heated at rates in the range 1-20 °C/s to 1200 °C and quenched at 10 °C/s. Phase transformations were detected by monitoring the fractional change in dilatation with temperature.

## 3. PHASE STABILITY CALCULATIONS

The phase diagram calculations revealed significant differences between the three alloys. The most dominant equilibrium carbide was in all cases found to be $M_{23}C_6$. This was the sole alloy carbide for steel 3, whereas $M_2C$ and $M_3C$+$M_7C_3$ could coexist with $M_{23}C_6$ in steels 2 and 1 respectively. The mole percent of each phase, along with the partition of the alloying elements in each phase, is given in for the three steels in tables 2-4.

| Phase | Mole % | Composition (mole fraction) | | | | | | | |
|---|---|---|---|---|---|---|---|---|---|
| | | Fe | Cr | Mn | Ni | Mo | V | Si | C |
| Ferrite | 93.5 | 0.955 | 0.001 | 0.002 | 0.033 | - | 0.002 | 0.005 | - |
| $M_3C$ | 1.3 | 0.600 | 0.075 | 0.064 | 0.011 | - | - | - | 0.250 |
| $M_7C_3$ | 1.1 | 0.270 | 0.313 | 0.113 | - | 0.004 | - | - | 0.300 |
| $M_{23}C_6$ | 4.1 | 0.605 | 0.099 | - | - | 0.090 | - | - | 0.207 |

Table 2. Composition and mole % of equilibrium carbides in steel 1 at 560°C.

| Phase | Mole % | Composition (mole fraction) | | | | | | | |
|---|---|---|---|---|---|---|---|---|---|
| | | Fe | Cr | Mn | Ni | Mo | V | Si | C |
| Ferrite | 93.5 | 0.961 | 0.002 | - | 0.036 | - | - | 0.001 | - |
| $M_2C$ | 0.6 | 0.002 | 0.326 | 0.002 | - | 0.044 | 0.292 | - | 0.333 |
| $M_{23}C_6$ | 5.9 | 0.589 | 0.115 | - | - | 0.090 | - | - | 0.207 |

Table 3. Composition and mole % of equilibrium carbides in steel 2 at 560°C.

| Phase | Mole % | Composition (mole fraction) | | | | | | | |
|---|---|---|---|---|---|---|---|---|---|
| | | Fe | Cr | Mn | Ni | Mo | V | Si | C |
| Ferrite | 91.5 | 0.956 | 0.002 | - | 0.038 | - | 0.003 | 0.001 | - |
| $M_{23}C_6$ | 8.5 | 0.559 | 0.131 | - | - | 0.103 | - | - | 0.207 |

Table 4. Composition and mole % of equilibrium carbides in steel 3 at 560°C.

The $M_{23}C_6$ carbide is therefore the most dominant precipitate under equilibrium conditions, but is unlikely to form immediately at 560 °C due to a large activation energy for nucleation.It generally forms through a precipitation sequence involving $M_3C$ and $M_7C_3$ [4]. In the meantime, other carbides can precipitate and the identity of these carbides can sometimes be revealed by suppressing the $M_{23}C_6$ phase in the calculations to give the next most thermodynamically stable carbide. Tables 5-7 give the results of the calculations for each steel at 560 °C for the case where $M_{23}C_6$ is suppressed. The calculations were also carried out over a temperature range of 500-700 °C, typical of that used for the tempering of high strength steels; those results are illustrated in Figs.1-3.

| Phase | Mole % | Composition (mole fraction) | | | | | | | |
|---|---|---|---|---|---|---|---|---|---|
| | | Fe | Cr | Mn | Ni | Mo | V | Si | C |
| Ferrite | 94.6 | 0.957 | 0.001 | 0.001 | 0.033 | - | 0.002 | 0.005 | - |
| $M_3C$ | 1.9 | 0.643 | 0.058 | 0.034 | 0.010 | 0.004 | - | - | 0.250 |
| $M_7C_3$ | 3.5 | 0.302 | 0.223 | 0.074 | - | 0.101 | - | - | 0.300 |

Table 5. Composition and mole % of equilibrium carbides in steel 1 at 560 °C, in the absence of $M_{23}C_6$.

| Phase | Mole % | Composition (mole fraction) | | | | | | | |
|---|---|---|---|---|---|---|---|---|---|
| | | Fe | Cr | Mn | Ni | Mo | V | Si | C |
| Ferrite | 94.7 | 0.960 | 0.001 | - | 0.035 | - | 0.002 | 0.001 | - |
| $M_3C$ | 2.0 | 0.668 | 0.066 | 0.001 | 0.010 | 0.005 | - | - | 0.250 |
| $M_7C_3$ | 2.9 | 0.313 | 0.272 | 0.002 | - | 0.113 | - | | 0.300 |
| $M_6C$ | 0.4 | 0.338 | 0.007 | - | - | 0.512 | - | - | 0.143 |

Table 6. Composition and mole % of equilibrium carbides in steel 2 at 560 °C, in the absence of $M_{23}C_6$.

| Phase | Mole % | Composition (mole fraction) | | | | | | | |
|---|---|---|---|---|---|---|---|---|---|
| | | Fe | Cr | Mn | Ni | Mo | V | Si | C |
| Ferrite | 93.5 | 0.958 | 0.001 | - | 0.037 | - | 0.002 | 0.001 | - |
| $M_3C$ | 1.7 | 0.667 | 0.066 | 0.002 | 0.011 | 0.005 | - | - | 0.25 |
| $M_7C_3$ | 4.0 | 0.313 | 0.267 | 0.005 | - | 0.115 | - | - | 0.300 |
| $M_6C$ | 0.8 | 0.338 | 0.007 | - | - | 0.512 | - | - | 0.143 |

Table 7. Composition and mole % of equilibrium carbides in steel 3 at 560 °C, in the absence of $M_{23}C_6$.

It can be seen that in the absence of $M_{23}C_6$, the main carbides that form are $M_3C$ and $M_7C_3$, with some $M_6C$ in the more heavily alloyed steels 2 and 3. Of particular interest is the higher chromium and molybdenum concentrations in $M_7C_3$ compared to $M_3C$, and the very high molybdenum concentration in $M_6C$. Examination of the variation of carbide concentration with temperature (Figs.1-3) reveals an increase in the mole fraction of $M_3C$ with increasing tempering temperature, at the expense of the $M_7C_3$ carbide. Steels 2 and 3 would be expected to contain some $M_6C$ which is absent from steel 1, and both steel 1 and steel 2 have temperatures at which $M_2C$ is stable at the expense of $M_7C_3$, both carbides being molybdenum-rich. In all three steels the relative amounts of carbides are similar, but the striking difference is in the total carbide content, which is significantly higher in steel 3. This accounts immediately for the higher hardness of steel 3 after tempering (Fig.4).

## 4. MICROSCOPY

Transmission electron microscopy showed the microstructures of all three alloys to be similar, with little change in carbide size and distribution during tempering from 1 hour to 16 hours. Selected area diffraction patterns confirmed the presence of $M_3C$ and $M_7C_3$ carbides. Larger $M_{23}C_6$ particles were also identified, and diffraction studies indicated the presence of some $M_6C$, although this could not be identified

unambiguously. The $M_2C$ carbide was never positively identified using electron microscopy.

The carbides were found to adopt distinctive morphologies. $M_3C$ (orthorhombic, $a$=4.5241Å, $b$=5.0883Å, $c$=6.7416Å) occurred as elongated carbide plates aligned along <111> matrix directions, giving Widmanstatten-type arrays (Fig.5). $M_7C_3$ (trigonal, a=13.982Å, c=4.506Å) was present on a finer scale with a more rounded shape than the $M_3C$ carbide (Fig.6). The $M_7C_3$ carbide contained stacking faults along $\{10\bar{1}0\}$ planes, giving easily identifiable streaks on diffraction patterns. These streaks were not easily observed during thin foil transmission electron microscopy because of strong diffraction from the matrix, but were readily visible in carbon extraction replicas samples, where there is no background diffraction to mask the contributions form particles. All three steels also contain larger particles, typically on lath boundaries (Fig.7), which could be either $M_{23}C_6$ or $M_6C$, both carbides having face-centred cubic structures with similar unit cell parameters (10.638Å and 11.082Å respectively). As stated above, $M_2C$ (hexagonal, a=3.002Å, c=4.506Å) was never positively identified using electron diffraction. This carbide usually forms as needles aligned with <100> directions, giving a distinctive perpendicular array of fine carbides. Although not extensive, such an array has been observed in steel 2 (Fig.8) but is not representative of the main carbide form.

Microanalysis of carbides was carried out using energy dispersive X-ray analysis (EDX) on carbon extraction replicas of steel 1 tempered for 2 hours. Preliminary results suggest that both rounded and aligned particles appear to have similar compositions, with chromium contents in the range 3-6 weight % and molybdenum contents in the range 4-20 weight %, with molybdenum consistently having a greater concentration than chromium. These compositions discount $M_2C$, which has a significant vanadium content, $M_3C$, which contains very little molybdenum, *and* $M_6C$, which contains very high levels of molybdenum (tables 2-4). It is unlikely that $M_{23}C_6$ forms after 2 hours of tempering so the carbides are most probably $M_7C_3$, as suggested by diffraction studies.. This carbide usually has a much higher chromium content (see table 2) but after only 2 hours of tempering the equilibrium solute concentrations within carbides are unlikely to have developed.

## 5. TRANSFORMATION TEMPERATURES

The austenite start and finish temperatures, $Ac_1$ and $Ac_3$, and the martensite start temperature, $M_s$, were determined experimentally using a *ThermecMastor* thermomechanical simulator. The variation in specimen dimensions with temperature during both heating and cooling is shown in Fig. 9. The transformation temperatures are defined as the points where the curve leaves the tangent to the linear portion. The variation in $Ac_1$ and $Ac_3$ with heating rate for the three steels is given in table 8.

| Heating | Steel 1 | | Steel 2 | | Steel 3 | |
|---|---|---|---|---|---|---|
| rate °C/s | $Ac_1$ (°C) | $Ac_3$ (°C) | $Ac_1$ (°C) | $Ac_3$ (°C) | $Ac_1$ (°C) | $Ac_3$ (°C) |
| 1 | 724 | 776 | 734 | 778 | 737 | 786 |
| 10 | 752 | 806 | 766 | 819 | 769 | 833 |
| 20 | 752 | 823 | 763 | 840 | 769 | 847 |

Table 8. Start and finish temperature for the ferrite-austenite transformation on heating.

In all cases the transformation temperatures are highest for steel 3 and lowest for steel 1, reflecting the higher alloy content of steel 3. The $Ac_3$ temperature is more sensitive to both composition (steel type) and heating rate than the $Ac_1$ temperature, which notably shows no dependence on heating rate for 10 and 20 °C/s in all three steels.

The martensite start temperature for each steel, determined using a quench rate of 10°C/s, is given in table 9, along with theoretical values determined from calculations of the time-temperature-transformation (TTT) diagram based on the alloy composition [5]. Steel 3, with its higher carbon and alloy content, has a significantly lower $M_s$ temperature than the other two steels. Steel 2, with the lowest carbon content, has the highest $M_s$ temperature. In all three cases there is good agreement between theoretical and experimental values.

| | Steel 1 | Steel 2 | Steel 3 |
|---|---|---|---|
| Theoretical | 300 | 321 | 268 |
| Experimental | 290±5 | 310±10 | 275±10 |

Table 9. Theoretical and experimental values for martensite start temperature (°C).

# 6. DISCUSSION

It is evident that the tempering heat treatments used do not lead to the formation of the thermodynamically most stable carbide, $M_{23}C_6$, which forms as relatively coarse particles. However, finer intermediate carbides can precipitate during tempering, and for maximum strengthening effect it is important to obtain the optimum distribution of alloy carbides. In Cr-Mo-V steels the grteatest strengthening effect has been attributed to molybdenum and vanadium-rich $M_2C$ carbides forming in sheets of needles along <100> ferrite directions, with $M_7C_3$ and $M_3C$ having lesser strengthening effects [6]. However it is apparent both from thermodynamic modelling and transmission electron microscopy that for the alloy chemistries of the steels used in this study that the secondary hardening strengthening effect is due to the precipitation of $M_7C_3$ and $M_3C$ non-equilibrium carbides, and not to the precipitation of $M_2C$. Consequently the difference in strength levels between steel 3 and the other two steels is due to the greater mole fraction of carbides through its higher carbon and alloy concentration, and not to any difference in precipitation sequence as was originally suspected.

The dilatometry experiments provide important information for the heat treatment of these alloys. In all cases the austenite start temperature is above 700°C, which is considered the upper limit for tempering heat treatments. The development of austenite during tempering would alter the microstructure and have deleterious effects upon the mechanical properties of tempered steels. The austenite finish temperature is a maximum at 847°C in steel 3, which again defines a limit for the austenisation temperature of these steels. Above 900°C, the grain boundary pinning particles $V_4C_3$ start to dissolve, leading to austenite grain growth and subsequent deleterious effects on mechanical properties. Therefore austenisation is best carried out between 850°C and 900°C. The good agreement between experimental and theoretical martensite start temperatures is encouraging, and further work aims to consider the sensitivity of martensite and bainite formation to cooling rate, which is of importance in the quenching and tempering of large sections where cooling rates are non-uniform across the section.

## 7. CONCLUSIONS

Thermodynaimc modelling predicts the formation of $M_{23}C_6$ as the most stable carbide during tempering of three Cr-Mo-V steels at 560 °C. It also predicts the precipitation of $M_7C_3$ and $M_3C$ as the principal non-equilibrium carbides. $M_2C$ is not predicted at 560 °C, although it is stable at various temperatures in the range 500-700°C for steels 1 and 2. Thin foil transmission electron microscopy confirms the findings of the thermodynamic modelling with a fine distribution of $M_7C_3$ and Widmanstatten arrays of $M_3C$. There is little difference in the carbide distributions of the three steels, and the greater secondary haredening response of steel 3 is accounted for by its higher carbon and alloy content giving a greater mole fraction of carbides. Microanalysis of $M_7C_3$ carbides after 2 hours of tempering suggests that carbide composition is non-equilibrium. Dilatometry has confirmed the austenite and martensite transformation temperatures, the latter agreeing with theoretical values. These values give safe limits for suitable secondary hardening heat treatments.


## ACKNOWLEDGEMENTS

This paper descibes work supported by the Defence Research Agency, Fort Halstead, Kent. The authors would like to thank Prof. C.J.Humphreys for the provision of research facilities.


## REFERENCES


[1] 'R. W. K. Honeycombe and H.K.D.H.Bhadeshia, Steels: Microstructure and properties, 2nd edition, Edward Arnold, London, 1995.

[2] C. J. McMahon, Jr., Innovations in Ultrahigh-strength Steel Technology, eds. G. B. Olson, M. Azrin and E. S. Wright, published by the U. S. Army Materials Laboratory Command, New York, 1987, pp. 597-618.

[3] MTDATA - Metallurgical and Thermochemical Data, National Physical Laboratory, Teddington, Middelsex, U. K., 1994.

[4] R. G. Baker and J. Nutting, J.I.S.I., **192**, pp. 257-268, 1959.

[5] H.K.D.H.Bhadeshia, Metal Science, **15**, pp.178-180, 1981

[6] F. B. Pickering, Physical Metallurgy and the Design of Steels, Applied Science Publishers, Essex, U.K., p. 133, 1978.

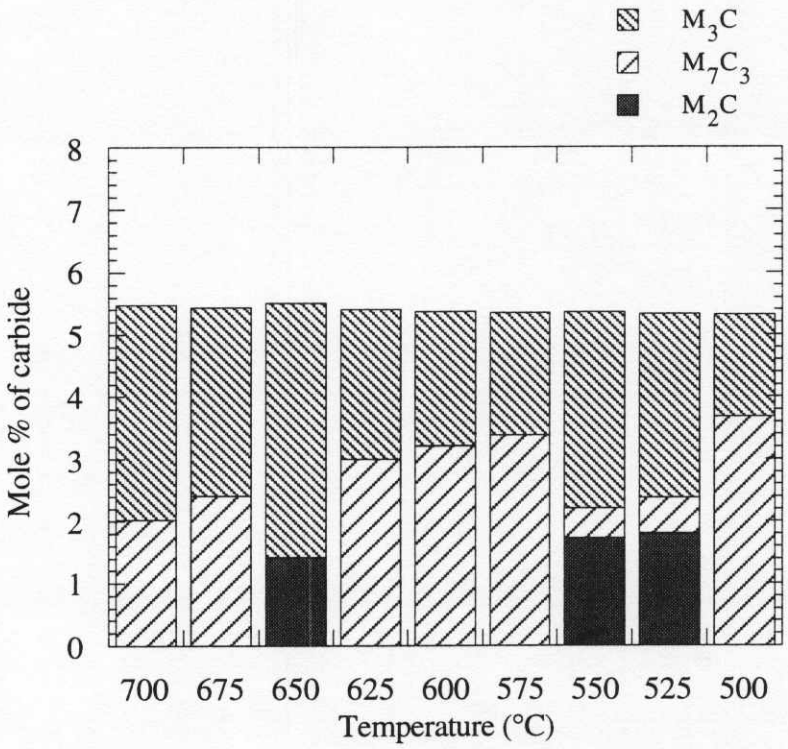


Fig.1. Mole % of carbides in Steel 1 in the absence of $M_{23}C_6$.

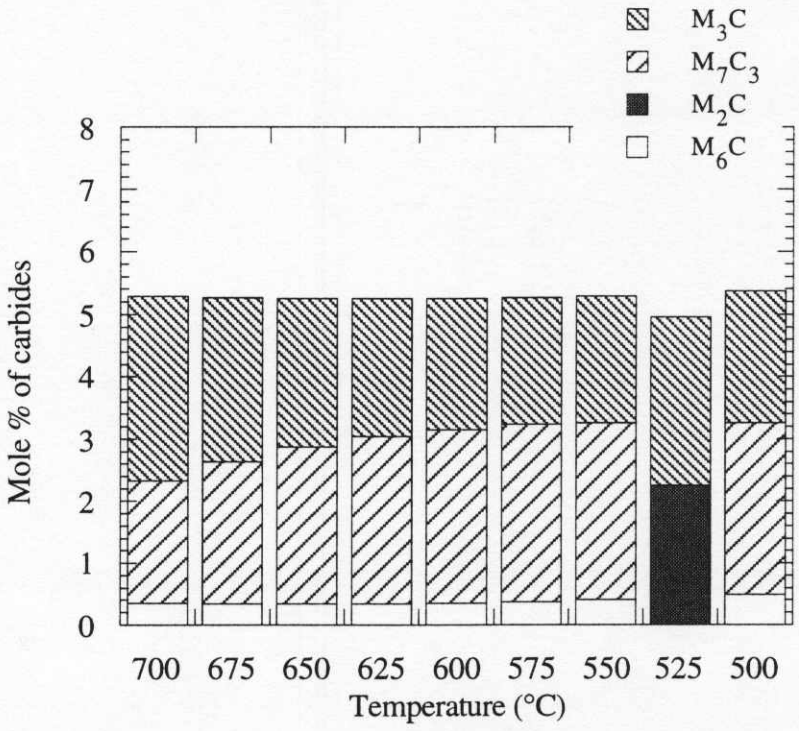


Fig. 2. Mole % of carbides in steel 2 in the absence of $M_{23}C_6$.

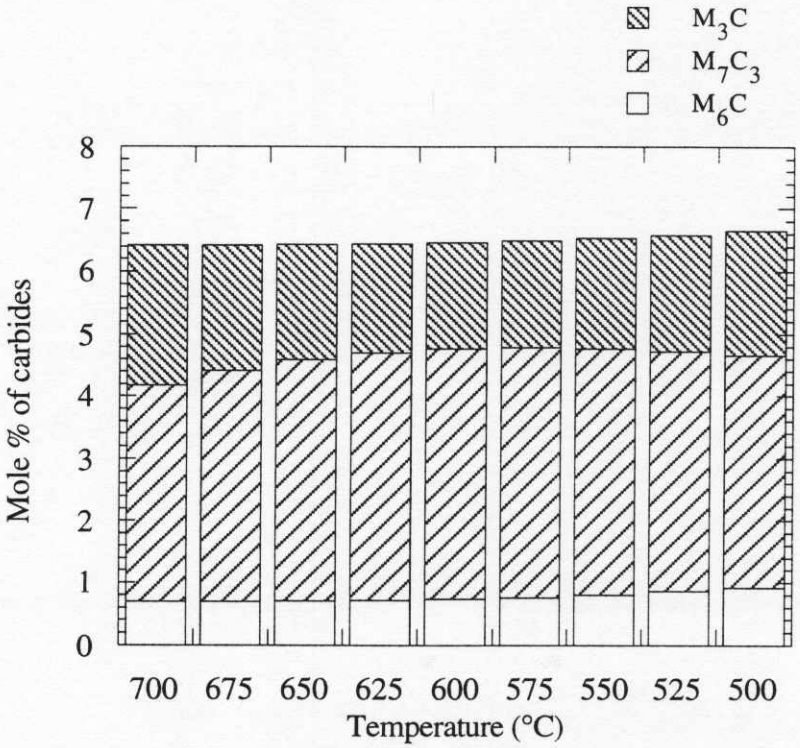


Fig.3. Mole % of carbides in Steel 3 in the absence of $M_{23}C_6$.

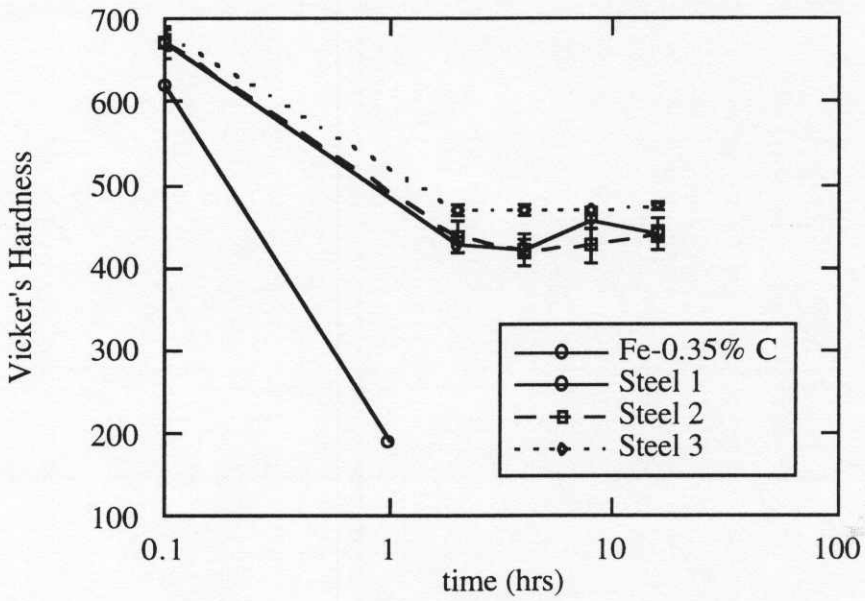


Fig. 4. Variation of hardness with tempering time at 560°C.

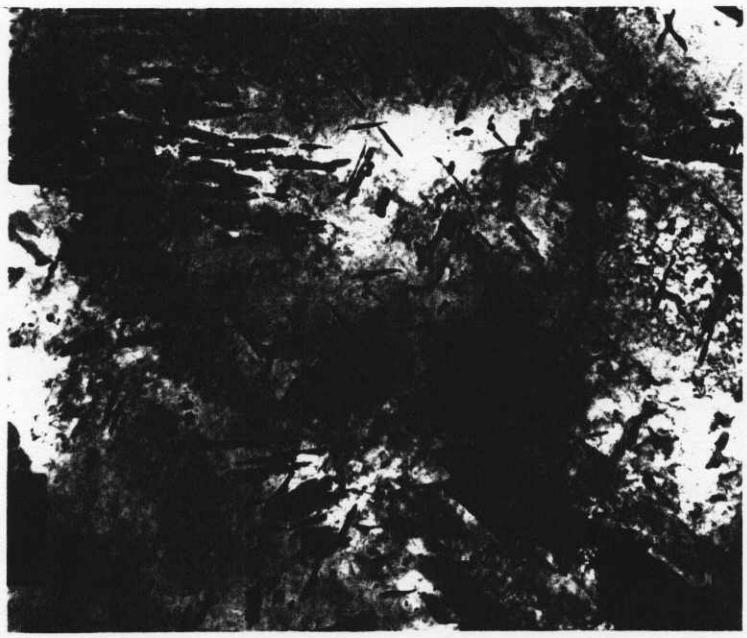

0.5µm

Fig.5. $M_3C$ carbides in steel 2, after tempering for 2 hours at 560°C.


Fig.6. $M_7C_3$ carbides in steel 2, tempered for 16 hours at 560°C.


Fig. 7. Lath boundary carbides in steel 2, tempered for 2 hours at 560°C.

0.3μm

Fig.8. Orthogonal carbides in steel 2, tempered for 16 hours at 560°C.

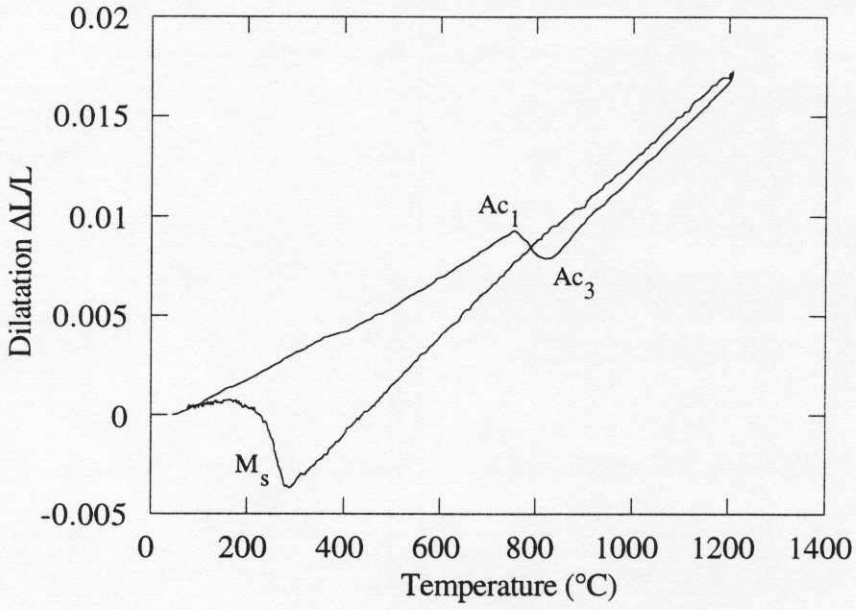


Fig.9. Actual dilatation variation with temperature on heating and cooling between room temperature and 1200°C, in steel 1 heating at 20°C/s and cooling at 10°C/s.